

HARMONIC GENERATION FEL MAGNETS: MEASURED B-FIELDS COMPARED TO 3D SIMULATIONS

W. S. Graves, L. Solomon, Brookhaven National Laboratory, Upton, NY 11973 USA

The Harmonic Generation Free Electron Laser [1] is a short period, high-gain amplifier FEL configured as an optical klystron. It is designed to lase at $3.47\mu\text{m}$ using a 30 MeV electron beam at the Accelerator Test Facility at BNL. Each of the three superconducting wiggler magnet sections (modulator, dispersion, radiator) has been built and the magnetic fields have been measured. This paper compares the measurement results with three-dimensional nonlinear computer models created with the TOSCA code.

I. Introduction

The HGFEL currently under construction at BNL will lase on the 3rd harmonic of a conventional CO_2 seed laser. The wiggler is split into 3 sections. The first section (modulator) energy-modulates the electron beam in resonance with the fundamental wavelength of the seed laser. Following this, the dispersive section causes the energy modulation to become spatial bunching (also at the fundamental). Finally the bunched beam enters the radiator which is tuned to the 3rd harmonic and lases.

HGFEL Wiggler Parameters			
	Modulator	Dispersive	Radiator
Period (cm)	2.6	—	1.8
a_w	1.35	—	0.6
B-field (T)	0.79	0.81	0.51
N poles	24	5	168
Gap (mm)	8.6	8.6	6.0

The computer models were created with the finite-element program TOSCA [2]. The primary goals of the computer simulations of the magnets are to:

1. Predict the current excitation necessary to reach the desired magnetic fields.
2. Design the appropriate magnet end winding configuration so that the electron beam is not steered when the iron is saturated.
3. For the dispersion section, design the yokes and coils to give the full range of dispersion needed without introducing beam steering.

II. Modulator Magnet

The modulator magnet is machined from a single iron yoke. It has 12 2.6 cm periods. The operating current is 80 Amps through 96 turns in each main coil. The peak magnetic field is 7900 gauss. The entrance and exit windings use the lowest order binomial transition [3]. There are 1/4" thick field clamps at each end of the yoke to ensure that the magnetic scalar potential is zero there. In addition to the main windings, there are two sets of trims at each end to perform steering correction [4] (Fig. 1).

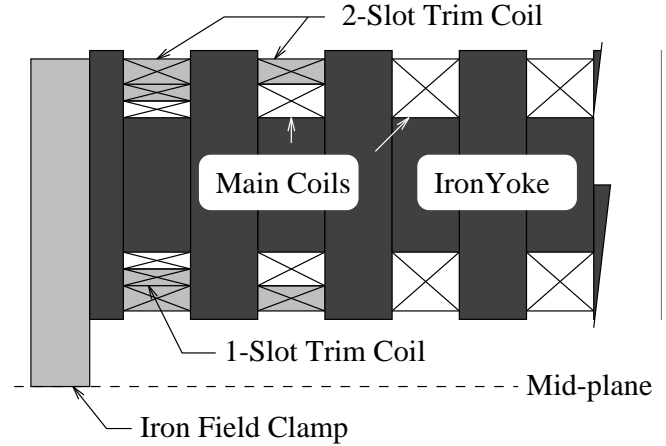


Figure 1. One end of the modulator magnet section, showing the main coil and trim winding configuration.

The trims are necessary because the steel in the nominally 1/2-strength pole at each end are less saturated than the full-strength poles, leading to an error in the magnetic scalar potential at that point. The optimum trim configuration has been found to be as shown, where 2 coils in series on either side of the 1/2-strength pole buck the main field, and 1 coil in the last slot provides fine adjustment. Typical trim strengths are 530 Amp-turns in the 2-slot trim and the 1-slot trim off when the main coils are at their operating value. Note that when the main coils are set at low enough current, the iron is unsaturated, and the trims are unnecessary. In the future it would be advantageous to design the number of turns in the last slots to account for the saturation at the operating point so that only very small corrections are required.

Using appropriate boundary conditions, the entire magnet may be modelled using just one octant of the 3D space containing the real magnet and surrounding air. Nonlinear saturation is taken into account using a B-H lookup table, and iteratively solving until a predefined maximum change in the solution at any node is achieved. The model contained 55×10^3 nodes, and takes about 8 cpu-hours to execute on an IBM RS6000/370. Figure 2 shows the measured B-fields and its second integral (equivalent to the electron trajectory) for the modulator. The mean peak field is 7787 gauss with RMS variation of just 0.2%. The peak fields in the simulation agree with the measured value to within 0.8%. The simulated fields are not shown in the figures because the differences from the measured values are indistinguishable on this scale. Of particular interest is the behavior near the magnet ends. Figure 3 shows the 2nd integral of the B-field for the modelled and measured fields with trims off. The difference in deflection angles is less than $1.0\mu\text{rad}$. The close agreement indicates that the model accurately predicts the level

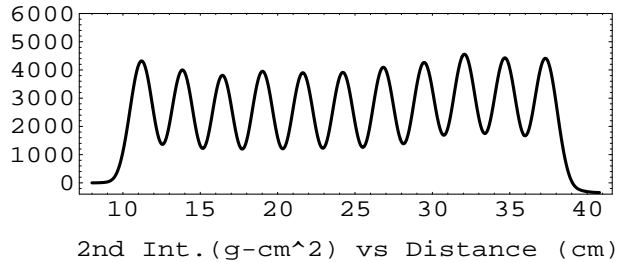
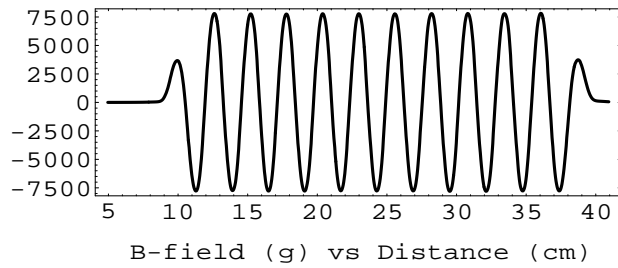


Figure 2. Measured B-fields and second integral for the modulator section. Main coils at 80 Amps, trims at 22 Amps. RMS variation among peaks is 0.2%.

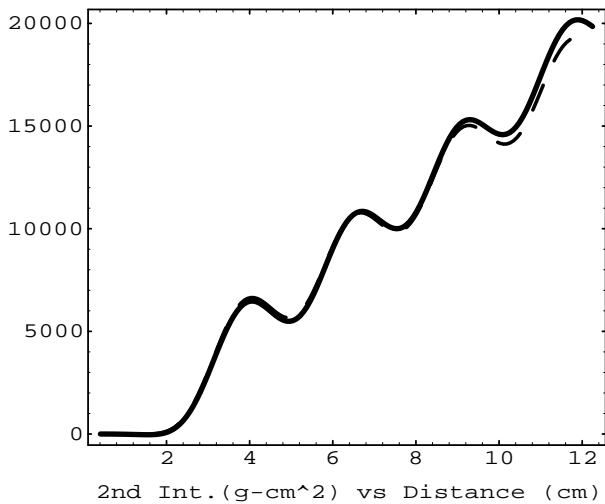


Figure 3. Measured (solid line) and modelled (dashed line) 2nd integrals of the modulator B-field at the entrance of the modulator. Main coils at 80 Amps, trims off.

of saturation and necessary trim correction.

III. Dispersion Magnet

The dispersion magnet (Fig. 4) is spaced 5cm downstream from the modulator. It has just 3 excited poles with a total length of 120 cm. The winding scheme is 23–147–147–23 turns. There is a trim coil to compensate for beam steering. Here, dispersion means change in longitudinal phase ψ with energy γ . The dispersion relation is approximately [5]

$$\frac{d\psi}{d\gamma} = \frac{k_s e^2}{m^2 c^2 \gamma^3} \int_0^L dz \left[\int_0^z dz' B_y(z') \right]^2 \quad (1)$$

where k_s is the radiation wavenumber. It is important that the dispersion be adjustable over as wide a range as possible to

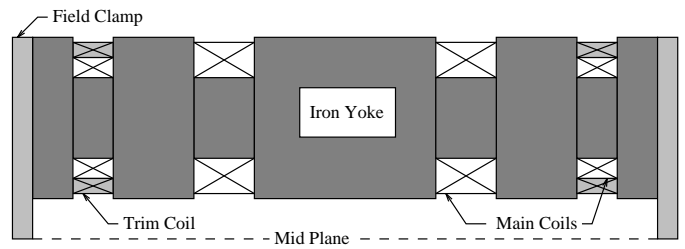


Figure 4. Dispersion magnet showing main and trim coils.

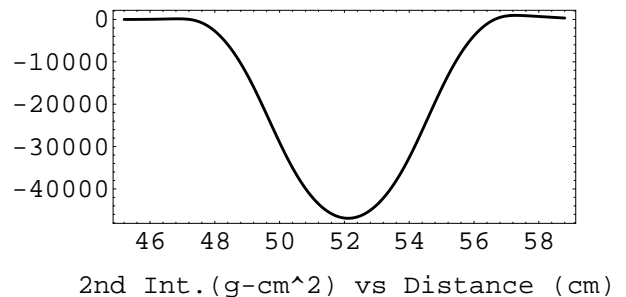
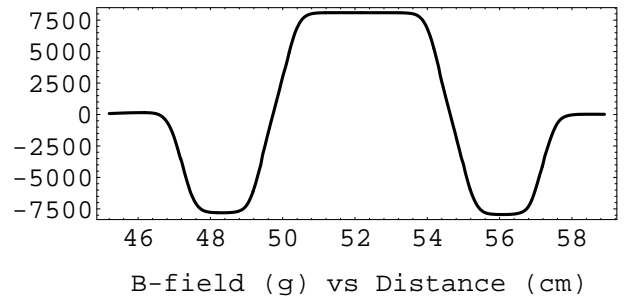


Figure 5. Measured B-field and 2nd integral for the dispersive section. Main coils at 100 Amps, trim coil at 8.5 Amps.

investigate the effect of varying the bunching on the laser performance.

The computer model is again one octant of the three dimensional space containing the iron and surrounding air plus the appropriate boundary conditions. It contains 59×10^3 nodes, and takes about 2.7 cpu-hours to solve. The execution time is reduced substantially from the modulator magnet because there are fewer coils. The time scales linearly with the number of coils.

The magnet was originally designed based on results from POISSON, a 2D magnetostatic solver. The 3D simulation results (obtained after the iron was cut) differed dramatically from the 2D because the finite size in the excluded dimension (transverse horizontal) severely limits the cross-sectional area available for flux transport in the iron. Thus the iron is far more saturated than predicted by the 2D model. The final coil configuration was modified based on the 3D results, and the measurements show very good agreement with this model. The peak field in the simulation differs from the measurement by 0.3%. The peak magnetic field at 100 Amps is 8100 gauss and the maximum dispersion is limited to 34.

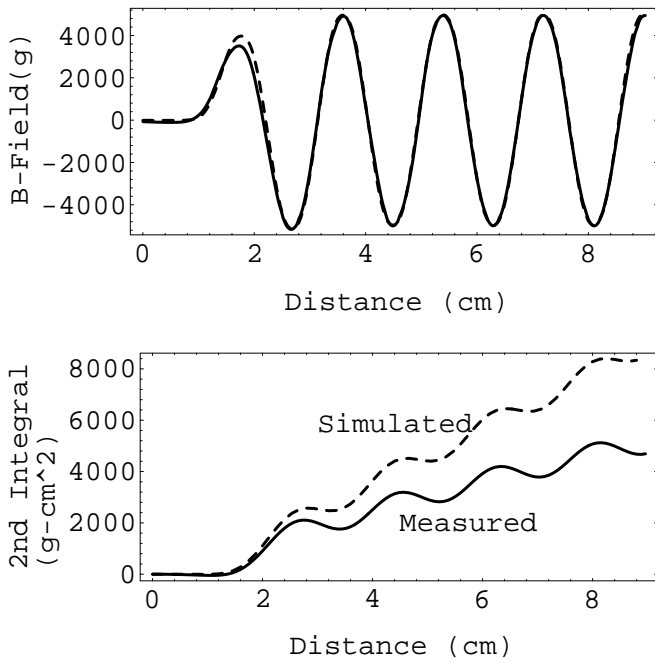


Figure 6. Measured (solid line) and simulated (dashed line) B-field and 2nd integral at the entrance of the radiator section. Main coils at 90 Amps, trim coils off.

IV. Radiator Magnets

The radiator section consists of six separate iron yokes, each with 18mm period, 0.51 Tesla peak magnetic field, and 6.1mm gap. Each yoke is physically very similar to the modulator magnet (Fig. 1) with two exceptions: the period is shorter, and the pole faces have a parabolic cut to provide horizontal electron beam focusing. The results of 3D simulations and measurements of the radiator magnets have been reported previously [4]. The earlier work studied the advantages of various entrance configurations of the coils in an effort to reduce the effects of saturation.

Figure 6 shows both the simulated and measured magnetic field and its 2nd integral at the entrance of the radiator section. The agreement between model and measurement is not as good as for the previous sections. There are several discrepancies between the computer model and the as-built configuration that may account for the disagreement. The model has a 5.6mm gap whereas the real magnet uses a 6mm gap. This changes the saturation in the iron and may account for different beam steering at the magnet entrance. The model also differs from the real magnet in that it has no parabolic pole face. A new simulation model is now being designed that matches the magnet as built. It is expected to perform as well as the modulator and dispersion section models.

V. Conclusions

Three dimensional simulations of each of the three distinct sections of a FEL configured as an optical klystron have been performed, and the results compared to measurements. These simulations include nonlinear saturation. The simulated on-axis magnetic fields for the modulator section agree with the measurements to 0.8%. Beam steering near the magnet entrance

due to iron saturation is also accurately modelled. For the dispersive section, simulation agrees with measurement to 0.3%. These results differ substantially from the 2D models because the limited cross-sectional area of the magnet changes the flux density in the iron. The radiator model does not yet perform as well and efforts are underway to gain better agreement with measurements.

VI. Acknowledgements

The authors would like to thank Bob Harrington and George Stenby for their technical assistance, and Ilan Ben-Zvi, Li-Hua Yu, and Sam Krinsky for their useful advice.

References

- [1] I. Ben-Zvi et al. Design of a harmonic generation fel experiment at bnl. *NIM A*, 318:208-211, 1992.
- [2] Vector Fields Limited, 24 Bankside, Kidlington, Oxford OX5 1JE, England. *OPERA-3d Reference Manual*, 1992.
- [3] K. Halbach. Desirable excitation patterns for tapered wigglers. *NIM A*, 250:95-99, 1986.
- [4] W.S. Graves, L. Solomon. End fields in the harmonic generation superconducting fel at bnl-nsls. *NIM A*, 358:414-417, 1995.
- [5] R. Bonifacio, R. Corsini, P. Pierini. Theory of the high-gain optical klystron. *Physical Review A*, 45(6):4091-4096, 1992.